Fully first-principles screened-exchange LDA calculations of excited states and optical properties of III-V semiconductors

S. H. Rhim, Miyoung Kim, and A. J. Freeman

Department of Physics & Astronomy and Materials Research Center, Northwestern University, Evanston, Illinois 60208, USA

Ryoji Asahi

Toyota Central R&D Laboratories, Inc., Nagauke, Aichi 480-1192, Japan
(Received 30 June 2004; published 5 January 2005)

Optical properties, such as the imaginary part of the dielectric function, index of refraction, reflectivity, and absorption coefficient, $[\varepsilon_2(\omega), n(\omega), k(\omega), R(\omega), \alpha(\omega)]$ of some III-V semiconductors (InAs, InSb, GaSb, and AlSb), are determined using our highly precise full-potential linearized augmented plane wave method with the screened-exchange local density approximation (sX-LDA) solved self-consistently and with spin-orbit coupling included. Here $\varepsilon_2(\omega)$ is calculated using the longitudinal expression with full $e^{i\mathbf{q} \cdot \mathbf{r}}$ matrix elements due to the nonlocality of the potential in the sX-LDA method, and its structure is analyzed with band structures and consideration of interband transitions. The critical point energies are also studied in comparison with experiment. The results of these fully first-principles calculations (no scissor operator or semiempirical inputs) show good agreement of the peak positions in $\varepsilon_2(\omega)$, $n(\omega)+ik(\omega)$, $R(\omega)$, $\alpha(\omega)$ and critical point energies with experiments.

I. INTRODUCTION

Since III-V semiconductors are important for their extensive applications as optoelectronic devices such as light emitting diodes and optosensors, it is of great importance to be able to accurately describe excitations by highly reliable and efficient *ab initio* approaches. As is well known, density functional theory[1,2] (DFT) has proven to be a very powerful tool for determining the electronic ground-state properties in a variety of materials. Although the local density approximation (LDA) has provided detailed calculations of the optical and dielectric properties based mostly on the independent-particle approximation,[3,4] its description of the excitation properties is questionable. The very well known band gap problem of LDA is the major challenge in the *ab initio* calculation of excitation energies,[5–7] since the optical properties determined in LDA still show large discrepancies from experiment

One approach to determine the optical properties theoretically is to model the dielectric function by adapting critical point energies from experiment.[8] The other approach uses the scissor approximation,[9,10] which displaces the eigenvalues of the unoccupied states by a rigid energy shift. The problem with this approximation is to find a more or less proper way to choose the shift of energy: one can adjust the eigenvalues so that the main peak of the imaginary part of the dielectric funcion corresponds to the transition energy $X_5^v \rightarrow X_1^c$ without spin-orbit coupling (SOC), or the $X_7^v \rightarrow X_6^c$ transition with SOC.[10] The resulting peak position is obtained considering only one k point in the Brillouin zone while the true contribution is rather spread out in the Brillouin zone.[14] Thus, it is also questionable whether the resulting eigenvalues thus shifted at other k points are the same as the experimental band structure. On the other hand, direct quasiparticle energies are available within the *GW*

approximation[15] and $\varepsilon_2(\omega)$ of Si was determined including excitonic and local-field effects by the *GW* approximation.[16] It was also shown that the existence of nonlocality in the self-energy makes the relation $\mathbf{v} = \mathbf{p}/m$ incorrect to ensure gauge invariance and charge conservation.[10,11]

Although the *GW* approximation removes most of the problems of LDA in treating excitation properties, its heavy computational demands have hampered determining properties self-consistently. A simplification of the *GW* approximation, called the model *GW*,[17,18] was proposed to reduce the numerical efforts associated with the *GW* approximation. The model *GW* has generally shown good agreement with experiment for nonmagnetic semiconductors using the pseudopotential method[17] and for transition-metal oxides[18,19] using the all-electron full-potential linearized augmented plane wave (FLAPW) method.[20] Although the model *GW* method is a promising scheme for various applications, the reliability of the calculated total energy, and, therefore, the ground states, has not been clearly shown.

The recently proposed screened-exchange LDA method[21,22] (sX-LDA) is one of the theories designed to find a better energy functional beyond LDA by modeling the exchange-correlation hole within *nonlocal* density schemes. The sX-LDA demonstrated encouraging results for the band gaps and structural properties of semiconductor materials with the plane-wave pseudopotential method[22] and the FLAPW method.[23] In particular, lattice constants obtained for Si, Ge, and GaAs show[22] better agreement with experiment than LDA, which indicates the ground states of sX-LDA are expected to be better than those of LDA. The advantage of sX-LDA over the *GW* approximation is that it is much less computationally demanding and it also enables the self-consistent determination of the ground state and excited properties and with full matrix elements for the optical properties. The recent work with sX-LDA using FLAPW demon-

strates very successful descriptions of excited states for pure semiconductors,[24] III-V semiconductors,[25] and heterostrucures.[26] The linear optical properties of Si, Ge, GaAs, and InSb was determined using self-consistent sX-LDA calculations,[24] as implemented in the FLAPW (Ref. 20) method with no adjustable parameters. Most recently, the sX-LDA approach has been successfully extended to the treatment of surfaces/interfaces and multilayers.[26]

In this paper, we report results of self-consistent sX-LDA plus spin-orbit coupling (SOC) calculations as implemented in the FLAPW method for the narrow band gap materials InAs, InSb, GaSb and AlSb. With self-consistent eigenvalues and wave functions and using the independent-particle approximation and no artificial parametrization, we determine the linear optical properties for these materials, namely the imaginary dielectric function, $\varepsilon_2(\omega)$, the index of refraction, $n(\omega)+ik(\omega)$, the reflectivity, $R(\omega)$, and the absorption coefficients, $\alpha(\omega)$, and make comparisons with experiment. We also demonstrate critical point energies obtained from the self-consistent sX-LDA plus SOC method which reveals the expected great improvement over the LDA.

II. SELF-CONSISTENT CALCULATION AND OPTICAL PROPERTIES

For our calculations, we employ the highly precise *ab initio* electronic structure FLAPW method with no artificial shape approximation for the wave functions, charge densities, and potentials. At first, the LDA-FLAPW is performed with the exchange-correlation potential using the Hedin-Lundvist parametrization[27] and cutoffs of the plane-wave basis (3.6 a.u. for InSb and 3.3 a.u. for the rest) and potential representation 8.0 a.u., and the expansion in terms of spherical harmonics with $l \leq 8$ inside the muffin-tin (MT) spheres. We used the experimental lattice constants for all materials: 11.45 (InAs), 12.24 (InSb), 11.51 (GaSb) and 11.59 (AlSb) in atomic units. With the converged LDA results, we performed sX-LDA plus spin-orbit coupling (SOC) calculations self-consistently with cut-off parameters of 3.1 a.u. in the wave vectors and $l \leq 4$ inside the MT spheres. Only s and p electrons were included in the screening. Summations over the Brillouin zone were done using ten special k points[28] in the irreducible wedge. Core states are treated fully relativistically and updated at each iteration, while the valence states are treated semirelativistically.

For the calculation of optical properties, the linear electronic response to a longitudinal external perturbation is described in the independent-particle approximation, or the random-phase approximation (RPA), by the dielectric matrix,

$$\varepsilon(\mathbf{q}+\mathbf{G},\mathbf{q}+\mathbf{G}',\omega)=\delta_{\mathbf{G},\mathbf{G}'}-V(\mathbf{q}+\mathbf{G})\chi_0(\mathbf{q}+\mathbf{G},\mathbf{q}+\mathbf{G}',\omega), \quad (1)$$

with $V(\mathbf{q})=4\pi e^2/q^2$, the Fourier representation of the Coulomb potential, and χ_0, the polarization function of the independent particle. Neglecting local-field effects, the imaginary part of the dielectric function in the long-wavelength limit, $q \to 0$, is written as

TABLE I. Band gaps (in eV) by LDA, sX-LDA plus SOC and experiment.

Band gap	InAs	InSb	GaSb	AlSb Indirect	AlSb Direct
LDA	−0.51[a]	−0.47[a]	−0.09	1.06	1.41
sX-LDA+SOC	0.35	0.11	0.43	1.53	2.11
Experiment[b]	0.42	0.24	0.82	1.69	2.38

[a]Reference 30.
[b]Data from Ref. 31.

$$\varepsilon_2(\omega)=\frac{8\pi^2 e^2}{V}\lim_{q\to 0}\sum_{c,v}\sum_{\mathbf{k}}\frac{1}{q^2}|\langle c,\mathbf{k}+\mathbf{q}|e^{i\mathbf{q}\cdot\mathbf{r}}|v,\mathbf{k}\rangle|^2$$
$$\times\delta[E_c(\mathbf{k}+\mathbf{q})-E_v(\mathbf{k})-\hbar\omega], \quad (2)$$

where c and v denote the conduction and valence bands, respectively. The direction of $\mathbf{q}$ defines one of the diagonal elements of the dielectric tensor, $\epsilon_{\alpha\alpha}$, which are all equal for cubic crystals. Taking the trace, therefore, makes it possible to restrict the calculations to the irreducible Brillouin zone (IBZ) defined by the crystal symmetry group. If we use the relation $\mathbf{p}/m=(i/\hbar)[H,\mathbf{r}]$, Eq. (2) is expressed as

$$\varepsilon_2(\omega)=\frac{8\pi^2 e^2}{\omega^2 m^2 V}\sum_{c,v}\sum_{\mathbf{k}}|\langle c,\mathbf{k}|\hat{\mathbf{e}}\cdot\mathbf{p}|v,\mathbf{k}\rangle|^2$$
$$\times\delta[E_c(\mathbf{k})-E_v(\mathbf{k})-\hbar\omega]. \quad (3)$$

The calculation using the transverse expression [Eq. (3)] is much faster than using Eq. (2) since only wave functions at the same $\mathbf{k}$ points of the conduction and valence bands are needed instead of pairs at $\mathbf{k}$ and $\mathbf{k}+\mathbf{q}$. However, as pointed out in Refs. 10–12, Eq. (3) is not correct when the Hamiltonian includes nonlocal potentials, as in the case of the sX-LDA method. Rather than the momentum operator, one needs to use the velocity operator defined by the Heisenberg equation of motion,

$$\mathbf{v}=\frac{d\mathbf{r}}{dt}=\frac{i}{\hbar}[H,\mathbf{r}]=\frac{\mathbf{p}}{m}+\frac{i}{\hbar}[v_{sx}^{\mathrm{NL}}(\mathbf{r},\mathbf{r}'),\mathbf{r}]. \quad (4)$$

Due to the nonlocality of the Hamiltonian with the sX-LDA approach, the gauge invariance requires the light-matter interaction in terms of $\mathbf{v}\cdot\mathbf{A}$ instead of $\mathbf{p}\cdot\mathbf{A}$,[11] since the transverse expression, Eq. (3), does not satisfy gauge invariance or equivalently charge conservation. Then it is easy to show

TABLE II. Critical-point energies (in eV) for InAs.

InAs	E_0	$E_0+\Delta_0$	E_0'	E_1	$E_1+\Delta_1$	E_2
LDA	−0.51		3.50	1.57		3.54
sX-LDA plus SOC	0.36	0.75	4.21	2.55	2.83	4.61
Expt. (Spitzer *et al.*[36])	0.42[a]			4.50	2.49	2.78	4.70
Adachi[8]	0.36	0.76		2.50	2.78	4.45

[a]From Ref. 31.
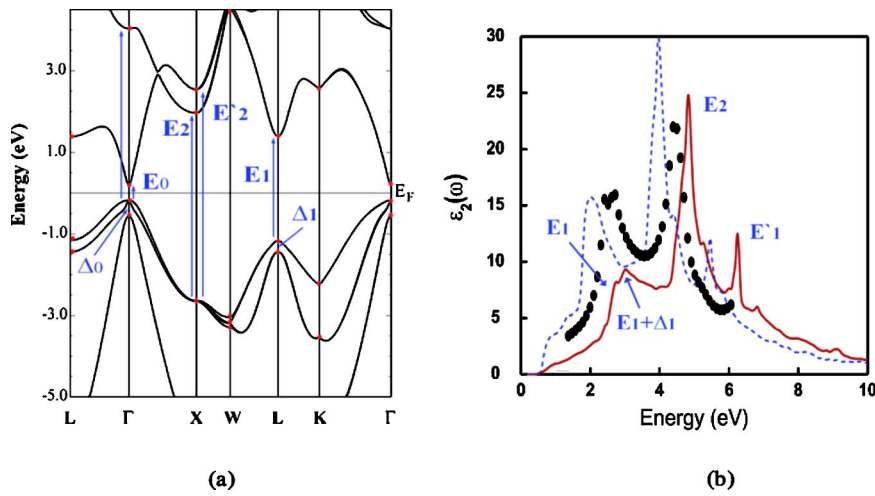
FIG. 1. (Color online) (a) Band structure of InAs. High symmetry points are shown in circles and important interband transitions are labeled as E_0: $\Gamma_8^v \rightarrow \Gamma_6^c$; E_0': $\Gamma_8^v \rightarrow \Gamma_7^c$; E_1: $L_{4,5}^v \rightarrow L_6^c$; $E_1 + \Delta_1$: $L_6^v \rightarrow L_6^c$; E_2: $X_7^v \rightarrow X_6^c$; and E_2': $X_7^v \rightarrow X_7^c$. (b) Imaginary dielectric constant. Solid line: sX-LDA plus SOC. Dashed line: LDA; filled circles: experiment (Ref. 33).
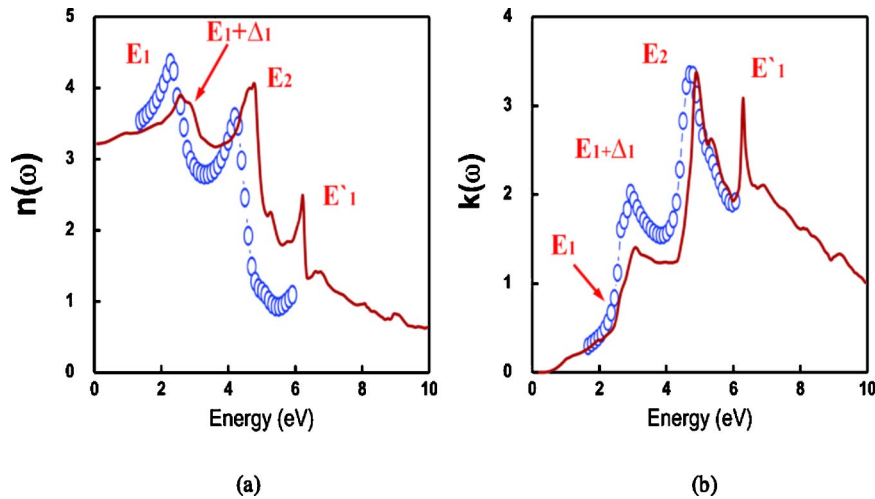
FIG. 2. (Color online) Index of refraction for InAs as a function of energy. (a) Real index of refraction $n(\omega)$ and (b) extinction coefficient $k(\omega)$. Solid line: this work. Open circles: experimental data by Aspnes et al. (Ref. 33).
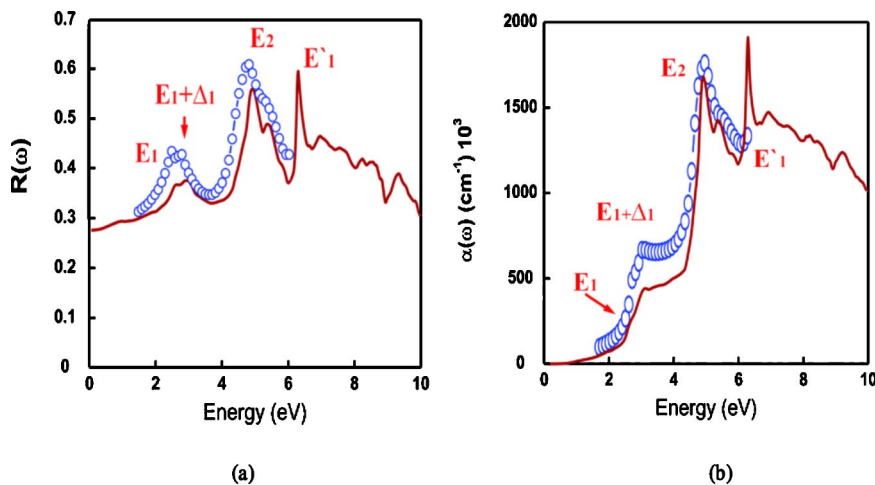
FIG. 3. (Color online) (a) Reflectivity $R(\omega)$ and (b) absorption coefficient $\alpha(\omega)$ of InAs as a function of energy. Solid line: this work. Open circles: experimental data by Aspnes et al. (Ref. 33).

(a)

(b)
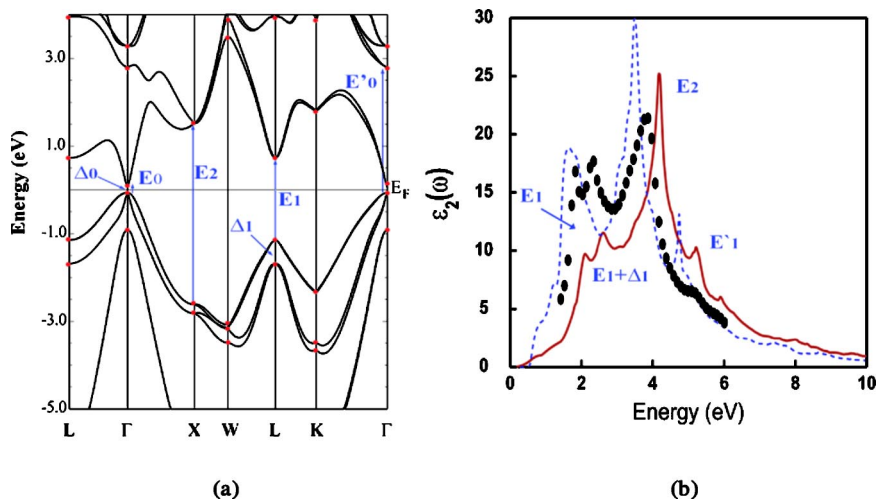
FIG. 4. (Color online) (a) Band structure of InSb. High symmetry points are shown in circles and important interband transitions are labeled as E_0: $\Gamma_8^v \rightarrow \Gamma_6^c$; E_0': $\Gamma_8^v \rightarrow \Gamma_7^c$; E_1: $L_{4,5}^v \rightarrow L_6^c$; $E_1 + \Delta_1$: $L_6^v \rightarrow L_6^c$; E_2: $X_7^v \rightarrow X_6^c$; and E_2': $X_7^v \rightarrow X_7^c$. (b) Imaginary dielectric constant. Solid line: sX-LDA plus SOC. Dashed line: LDA; filled circles: experiment (Ref. 33).

(a)

(b)
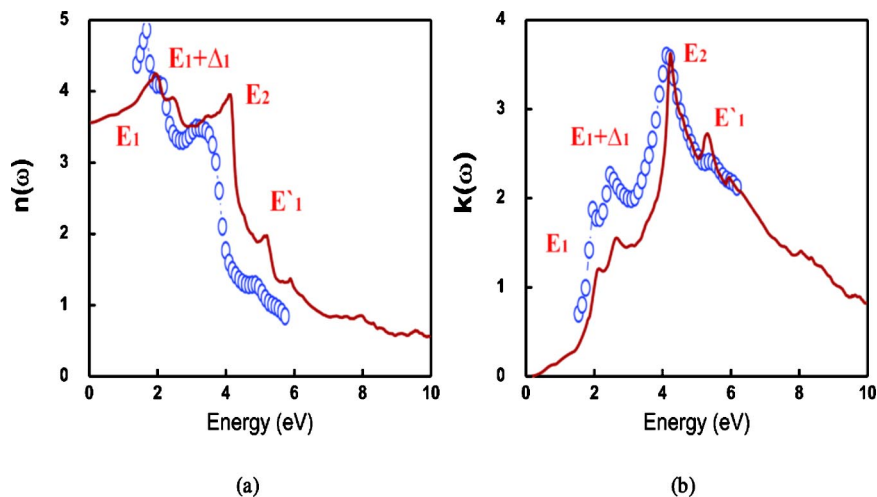
FIG. 5. (Color online) Index of refraction for InSb as a function of energy. (a) Real index of refraction $n(\omega)$ and (b) extinction coefficient $k(\omega)$. Solid line: this work. Open circles: experimental data by Aspnes *et al.* (Ref. 33).

(a)

(b)
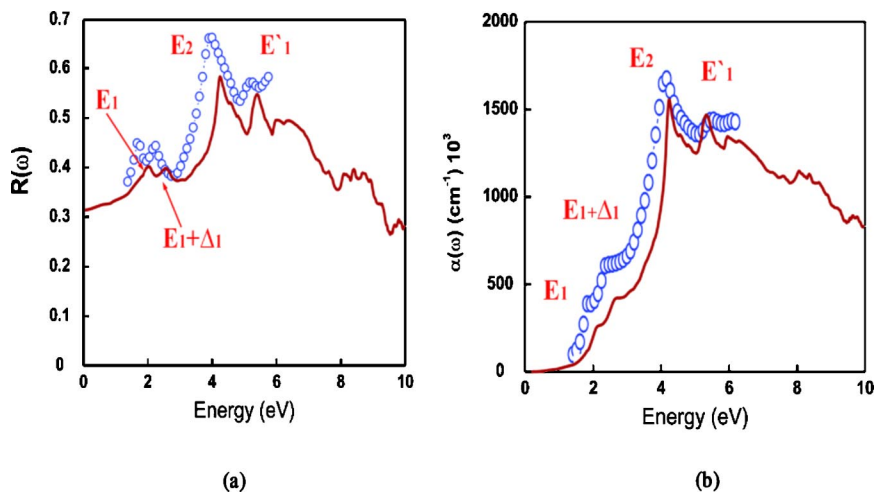
FIG. 6. (Color online) (a) Reflectivity $R(\omega)$ and (b) absorption coefficient $\alpha(\omega)$ of InSb as a function of energy. Solid line: this work. Open circles: experimental data by Aspnes *et al.* (Ref. 33).

TABLE III. Critical-point energies (in eV) for InSb.

InSb	E_0	$E_0+\Delta_0$	E_0'	E_1	$E_1+\Delta_1$	E_1'	E_2
LDA	−0.47		2.79	1.33		4.72	3.44
sX-LDA plus SOC	0.11	0.97	2.88	1.86	2.39	5.09	4.13
Expt. (Spitzer et al.[36])	0.23[a]		3.20	1.88	2.38		4.10
Adachi[32]	0.18	0.99	3.26	1.80	2.30	5.11	3.85

[a]From Ashcroft and Mermin (Ref. 31).

(a)

(b)
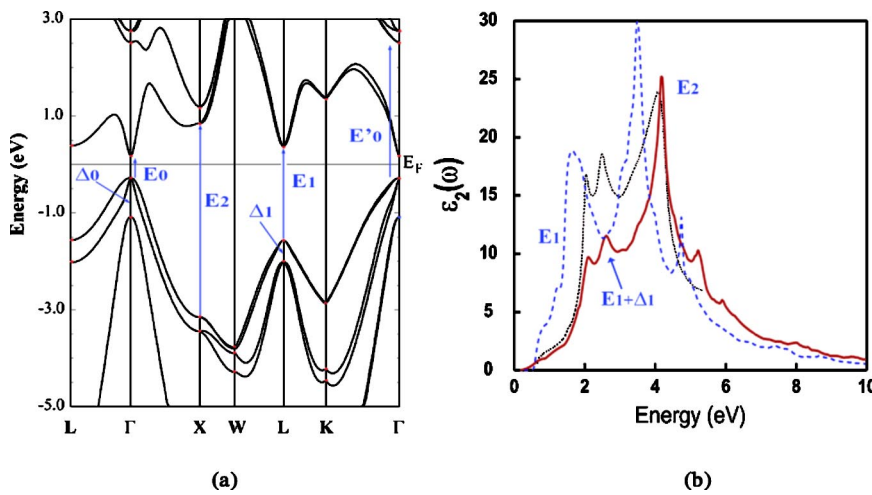
FIG. 7. (Color online) (a) Band structure of GaSb. High symmetry points are shown in circles and important interband transitions are labeled as E_0: $\Gamma_8^v \rightarrow \Gamma_6^c$; E_0': $\Gamma_8^v \rightarrow \Gamma_7^c$; E_1: $L_{4,5}^v \rightarrow L_6^c$; $E_1+\Delta_1$: $L_6^v \rightarrow L_6^c$; E_2: $X_7^v \rightarrow X_6^c$; and E_2': $X_7^v \rightarrow X_7^c$. (b) Imaginary dielectric constant. Solid line: sX-LDA plus SOC. Dashed line: LDA. Dotted line: experiment from Ref. 37.

(a)

(b)
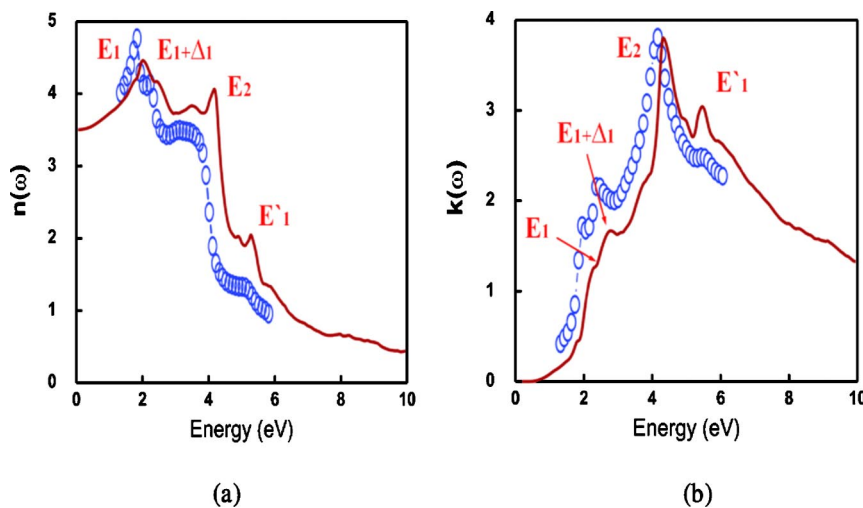
FIG. 8. (Color online) Index of refraction for GaSb as a function of energy. (a) Real index of refraction $n(\omega)$ and (b) extinction coefficient $k(\omega)$. Solid line: this work. Open circles: experimental data by Aspnes et al.[33]
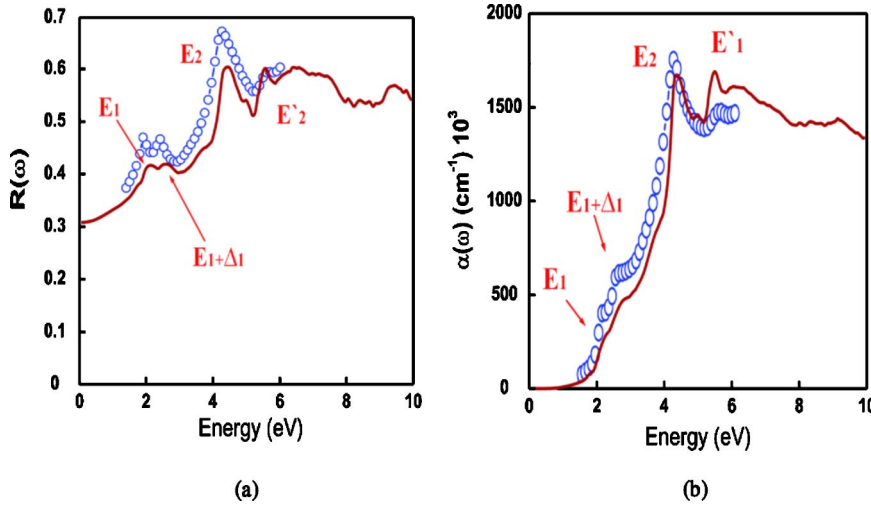
FIG. 9. (Color online) (a) Reflectivity $R(\omega)$ and (b) absorption coefficient $\alpha(\omega)$ of GaSb as a function of energy. Solid line: this work. Open circles: experimental data by Aspnes *et al.*[33]

that the dipole transition probability is equivalent to the longitudinal expression, Eq. (2), in the long-wavelength limit through the relation

$$i\langle c|[H,\mathbf{r}]|v\rangle = \lim_{q \to 0} \left(\frac{1}{q}\right)(E_c - E_v)\langle c|e^{i\mathbf{q}\cdot\mathbf{r}}|v\rangle. \quad (5)$$

In other words, Eq. (2) is appropriate whether the Hamiltonian is local or not, and so in this work the longitudinal expression [Eq. (2)] is employed. We calculated the optical properties using the self-consistent eigenvalues and wave functions obtained with the sX-LDA plus spin-orbit interaction. Once $\varepsilon_2(\omega)$ is obtained, we obtain the real part, $\varepsilon_1(\omega)$, by the Kramers–Kronig relation. Other quantities, the index of refraction $[n(\omega)+ik(\omega)]$, the reflectivity $[R(\omega)]$, and the absorption coefficient $[\alpha(\omega)]$, are obtained by the relations[13]

$$\varepsilon_1(\omega) = n(\omega)^2 - k(\omega)^2, \quad \varepsilon_2(\omega) = 2n(\omega)k(\omega),$$

$$R(\omega) = \frac{[n(\omega) - 1]^2 + k(\omega)^2}{[n(\omega) + 1]^2 + k(\omega)^2},$$

$$\alpha(\omega) = \frac{2\omega k(\omega)}{c}. \quad (6)$$

We found that 200 sampling k points in the irreducible wedge of the Brillouin zone are necessary for the narrow band gap semiconductors and used the linear analytic tetrahedron scheme[29] for the Brillouin zone integrations.

III. RESULTS

In Table I, we list calculated band gaps of InAs, InSb, GaSb and AlSb with LDA and sX-LDA plus spin-orbit coupling and compare with experiment. While LDA gives negative band gaps for InAs, InSb and GaSb, the sX-LDA plus SOC gives great improvement for the band gaps of these three materials. In addition, the sX-LDA plus SOC shows improvement not only for these direct band gap materials but also for indirect band gap materials for both their indirect and direct band gap, as is the case of AlSb. In the following

sections, we present band structures, imaginary dielectric constants, indices of refraction, reflectivities and absorption coefficients of InAs, InSb, GaSb, and AlSb. Also we discuss the CP energies obtained from sX-LDA plus SOC in comparison with CP energies from LDA, experiment and theoretical modeling by Adachi.[8,32] Adachi considered the following transition data from works by Aspnes *et al.*[33] and Seraphin *et al.*:[34] $\Gamma_8^v \to \Gamma_6^c (E_0$ transition), $\Gamma_8^v \to \Gamma_7^c (E_0'$ transition), $L_{4,5}^v \to L_6^c (E_1$ transition), $L_6^v \to L_6^c (E_1 + \Delta_1$ transition), and $X_7^v \to X_6^c (E_2$ transition). [$L_{4,5}^v \to L_{4,5}^c (E_1'$ transition) is considered for InSb.] For the description of these interband transitions, the labels follow Cardona's convention;[35] subscripts 0, 1, and 2 stand for transitions at Γ, L, and X in reciprocal space, respectively. Spin-orbit split energies are denoted as Δ. Since Umklapp processes are neglected in our work, this results in a systematically smaller magnitude of the E_1 peak in the imaginary dielectric function.

A. InAs

The calculated critical-point energies are given in Table II. While LDA underestimates all CP energies, the sX-LDA plus SOC gives excellent agreement with experiment.

The calculated band structure of InAs, with sX-LDA plus SOC, is shown in Fig. 1(a) where the important interband transitions are labeled and shown with vertical arrows. The imaginary dielectric function, $\varepsilon_2(\omega)$, is also shown in Fig. 1(b), which is obtained from the band structure with Eq. (2)

TABLE IV. Critical-point energies (in eV) for GaSb.

GaSb	E_0	$E_0+\Delta_0$	E_0'	E_1	$E_1+\Delta_1$	E_2
LDA	−0.09		2.71	1.44		3.41
sX-LDA plus SOC	0.43	1.23	3.04[a]	1.95	2.41	4.00
Expt. (Muñoz[37])	0.73	1.52	3.40	2.04	2.49	4.10
Adachi[8]	0.72	1.46		2.05	2.50	4.00

[a]$\Gamma_8^v \to \Gamma_8^c$ transition is considered.
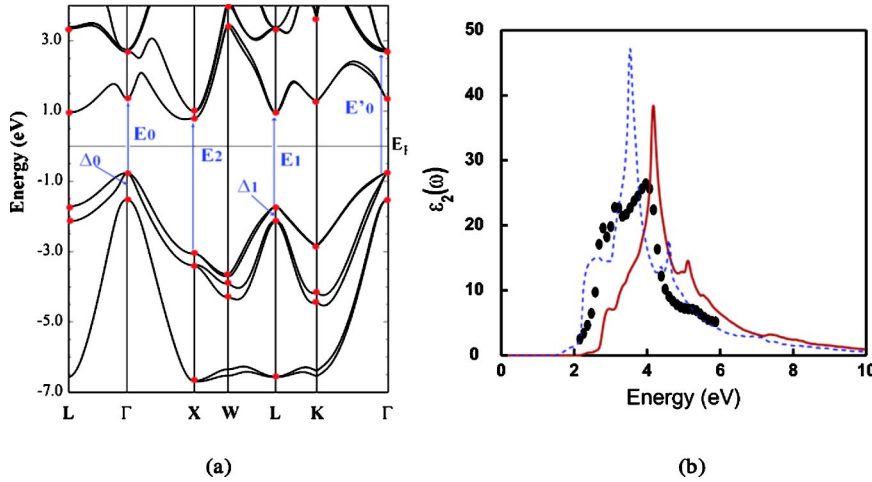
FIG. 10. (Color online) (a) Band structure of AlSb. High symmetry points are shown in circles and important interband transitions are labeled as E_0: $\Gamma_8^v \to \Gamma_6^c$; E_0': $\Gamma_8^v \to \Gamma_7^c$; E_1: $L_{4,5}^v \to L_6^c$; $E_1+\Delta_1$: $L_6^v \to L_6^c$; E_2: $X_7^v \to X_6^c$; and E_2': $X_7^v \to X_7^c$. (b) Imaginary dielectric constant. Solid line: sX-LDA plus SOC. Dashed line: LDA. Filled circles: experiment (Ref. 38).

(a)   (b)

using full matrix elements. Our results show a strong similarity of the peak structure with experiment. The E_2 peak, the transition from the valence band maximum (VBM) to the conduction band minimum (CBM) ($X_7^v \to X_6^c$), is 0.4 eV bigger than that of experiment. The $E_1+\Delta_1$ peak, the transition from the spin-orbit split band to the CBM ($L_6^v \to L_6^c$), is 0.2 eV bigger than that of experiment.[33] The shift in energy of the E_1 peak is thought to arise from exciton effects not considered here. Although the height is very small, our result also reproduces the E_1 peak, the transition $L_{4,5}^v \to L_6^c$.

The index of refraction is shown in Fig. 2. The peak positions of the real part in Fig. 2(a), $n(\omega)$, show the similar structure as $\varepsilon_2(\omega)$, and the extinction coefficient, $k(\omega)$, shows excellent agreement in their peak positions with experiment. Although the calculated E_1 and $E_1+\Delta_1$ peak heights are smaller than experiment, the main E_2 peak height shows good agreement with experiment.[33]

The reflectivity and absorption coefficient are plotted in Fig. 3. In both cases, our results show good agreement with experiment[33] in their peak positions as well as their peak heights.

B. InSb

Figure 4 presents our calculated (a) band structure and (b) imaginary dielectric constant for InSb, which has a smaller band gap than does InAs. In Fig. 4(a), we show the interband transitions, E_0, E_1, E_2, and E_0' and spin-orbit split energy at Γ, L, and X with Δ_0, Δ_1, and Δ_2. We find a similar peak structure to experiment, namely the clear structure of the E_1, $E_1+\Delta_1$ and E_2 peaks as in experiment. Here again the shift in energy of the E_1 peak is thought to arise from exciton effects not considered. They are 0.2 eV off from the experimental peak positions. The E_1' peak position matches experiment.

Figure 5 shows (a) the index of refraction $[n(\omega)]$ and (b) the extinction coefficient $[k(\omega)]$. The E_1, $E_1+\Delta_1$, and E_2 peak positions in $n(\omega)$ are off by 0.3 eV as they are in $\varepsilon_2(\omega)$, while the peak positions of our extinction coefficient, $k(\omega)$, match very well with experiment.

The reflectivity and absorption coefficient are presented in Fig. 6. As in the InAs case, the peak positions of our result show good agreement with experiment.

In Table III, we list the CP energies predicted by LDA and the sX-LDA plus SOC and those from experiment. The E_0' energy ($\Gamma_8^v \to \Gamma_7^c$ transition) by the sX-LDA plus SOC is off by 0.3 eV from experiment but sX-LDA plus SOC in general gives good agreement of the CP energies with experiment.

C. GaSb

Figure 7 shows our calculated (a) band structure and (b) imaginary dielectric function. The GaSb band structure shows a similar dispersion as the previous InAs and InSb results, except their curvature and enegy scales are different. We show interband transitions E_0, E_0', E_1, and E_2 at Γ, L, and X. Our $\varepsilon_2(\omega)$ shows excellent agreement with experiment[37] in their peak positions such as at the E_1, $E_1+\Delta_1$ and E_2 peaks. In this case, the experimental values reported have been obtained with exciton contributions excluded.

The index of refraction and extinction coefficient are presented in Fig. 8. We produced a structure similar to that in the dielectric function. As E_1' is off by 0.36 eV from experiment in $\varepsilon_2(\omega)$, it is also in both the real and imaginary index of refraction.

Figure 9 presents (a) the reflectivity and (b) the absorption coefficient. In both cases, we reproduced a peak structure similar to experiment. As in the case of the dielectric function, we see good agreement in the peak positions.

In Table IV, CP energies are listed as obtained by LDA, sX-LDA plus SOC and experiment. The CP energies at Γ calculated by sX-LDA plus SOC are systematically underestimated by $0.3-0.4$ eV compared to experiment. However, for the other transitions at L and X, the sX-LDA plus SOC gives good agreement with experiment.

TABLE V. Critical-point energies (in eV) for AlSb.

	E_0	E_0'	E_1	$E_1+\Delta_1$	E_1'	E_2
LDA	1.41	3.05	2.39		3.53	3.29
sX-LDA plus SOC	2.11	3.44	2.67	3.09	5.06	3.86
Expt. (Spitzer[36])		3.70	2.81	3.21		4.30
Expt. (Zollner et al.[38])	2.27	3.76	2.84	3.23	5.30	4.23
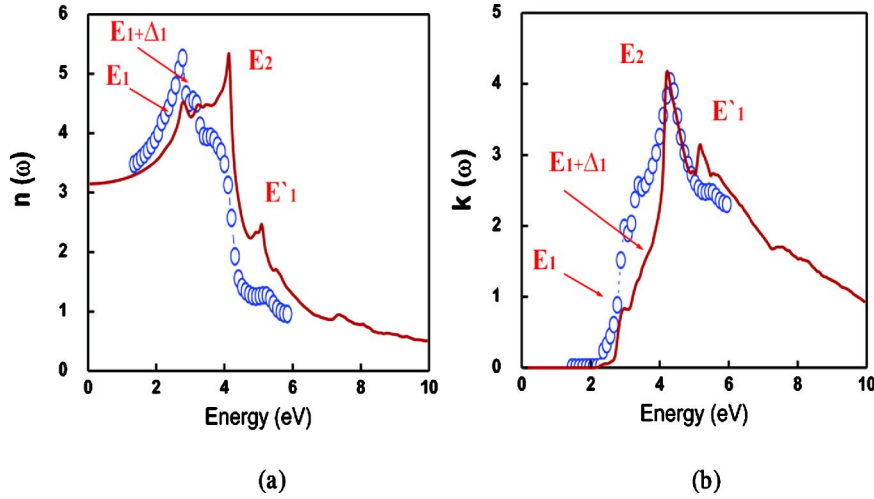
FIG. 11. (Color online) Index of refraction for AlSb as a function of energy. (a) Real index of refraction $n(\omega)$ and (b) extinction coefficient $k(\omega)$. Solid line: this work. Open circles: experiment (Ref. 38).

D. AlSb

AlSb is the only indirect gap material in our study. The band structure and imaginary dielectric constant are shown in Fig. 10. We see an indirect band gap from the VBM at Γ to the CBM at a point along the Γ-X direction. Again in the band structure, we denoted the interband transitions by E_0, E_1, and E_2 and the spin-orbit split energies by Δ_0 and Δ_1. The calculated $\varepsilon_2(\omega)$ shows an almost negligible effect of the indirect band gap. The peak positions of sX-LDA plus SOC show good agreement with experiment at $E_0+\Delta_0$, $E_1+\Delta_1$, E_2 and E_1' (cf. Table V).

The index of refraction $[n(\omega)]$ and the extinction coefficient $[k(\omega)]$ are shown in Fig. 11. In $n(\omega)$, the E_1 and $E_1+\Delta_1$ peak positions agree well with experiment although their heights are different. For the E_2 peak, where experiment shows a rather suppressed peak, there is, however, good agreement with experiment for its calculated position. However, the peak positions in $k(\omega)$ show generally good agreement with experiment, especially for the main E_2 peak.

Figure 12 presents (a) the reflectivity and (b) the absorption coefficient; excellent agreement with experiment is seen in their peak positions. Moreover, in the absorption coefficient, the E_2 peak shows a good match with experiment in both position and height.

We list CP energies in Table V determined by LDA, sX-LDA plus SOC and experiment. The sX-LDA plus SOC gives systematically lower values by 0.1–0.3 eV than experiment; however, we have a striking improvement over the LDA results given by sX-LDA plus SOC.

IV. SUMMARY AND CONCLUSION

We have presented results of fully first-principles calculations of the electronic structures and optical properties of InAs, InSb, GaSb, and AlSb as obtained with the sX-LDA plus spin-orbit coupling approach as implemented in the FLAPW method. The dielectric functions are evaluated with the longitudinal expression with full $e^{i\vec{q}\cdot\vec{r}}$ matrix elements. In general, comparisons with experiment show good agreement of our calculated dielectric functions in their peak positions. The sX-LDA plus SOC is found to give remarkable improvement over LDA in the critical-point energies and dielectric functions. The method employed to calculate the optical properties has the following features: (*i*) it is based *purely* on first-principles in that we do not use any artificial parameters to adjust the experimental results; it uses only the self-consistent eigenvalues and wave functions; (*ii*) the nonlocality of the Hamiltonian requires the longitudinal expression
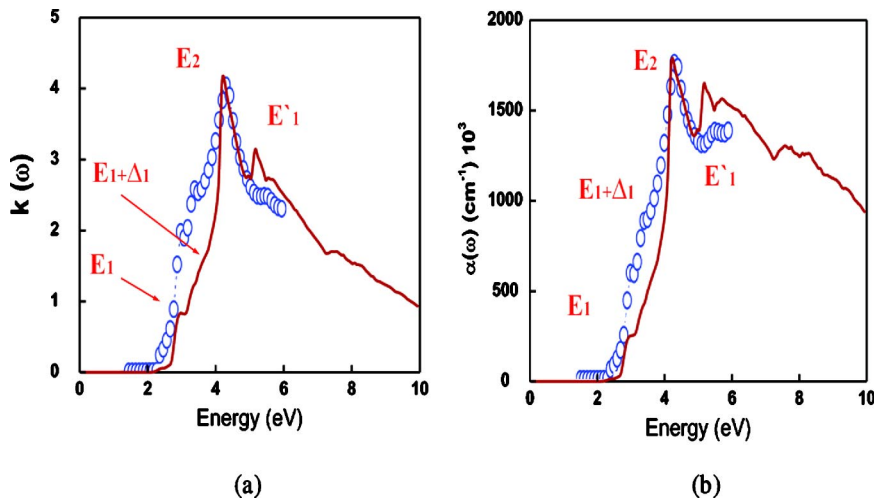
FIG. 12. (Color online) (a) Reflectivity $R(\omega)$ and (b) absorption coefficient $\alpha(\omega)$ of AlSb as a function of energy. Solid line: this work. Open circles: experiment (Ref. 38).

for the matrix elements. By comparison, using a scissor operator to shift the conduction bands rigidly does not guarantee preserving the band character at all k points; shifting the bands to match eigenvalues at one particular point does not neccessarily match the eigenvalue shift at all k points.

[1] P. Hohenberg and W. Kohn, Phys. Rev. **136**, B864 (1964).

[2] W. Kohn and L. J. Sham, Phys. Rev. **140**, A1133 (1965).

[3] H. Ehrenreich and M. H. Cohen, Phys. Rev. **155**, 786 (1959).

[4] G. Greenwood, Proc. Phys. Soc. London **71**, 585 (1958).

[5] S. B. Trickey, F. R. Green, Jr., and F. W. Averill, Phys. Rev. B **8**, 4822 (1973).

[6] J. P. Perdew and M. Levy, Phys. Rev. Lett. **51**, 1884 (1983).

[7] L. J. Sham and M. Schlüter, Phys. Rev. Lett. **51**, 1888 (1983); Phys. Rev. B **32**, 3883 (1985).

[8] S. Adachi, J. Appl. Phys. **66**, 6030 (1989).

[9] G. A. Baraff and M. Schlüter, Phys. Rev. B **30**, 3460 (1984).

[10] R. Del Sole and R. Girlanda, Phys. Rev. B **48**, 11 789 (1993).

[11] A. F. Starace, Phys. Rev. A **3**, 1242 (1971).

[12] Z. H. Levine and D. C. Allan, Phys. Rev. Lett. **63**, 1719 (1989).

[13] O. Madelung, in *Introduction to Solid-State Theory*, edited by M. Cardona, P. Fulde, and H.-J. Queisser (Springer, New York, 1996), p. 262.

[14] M. Alouani, L. Brey, and N. E. Christensen, Phys. Rev. B **37**, 1167 (1988).

[15] L. Hedin, Phys. Rev. **139**, A796 (1965).

[16] S. Albrecht, L. Reining, R. Del Sole, and G. Onida, Phys. Rev. Lett. **80**, 4510 (1998).

[17] F. Gygi and A. Baldereschi, Phys. Rev. Lett. **62**, 2160 (1989).

[18] S. Massidda, A. Continenza, M. Posternak, and A. Baldereschi, Phys. Rev. Lett. **74**, 2323 (1995).

[19] S. Massidda, A. Continenza, M. Posternak, and A. Baldereschi, Phys. Rev. B **55**, 13 494 (1997).

[20] E. Wimmer, H. Krakauer, M. Weinert, and A. J. Freeman, Phys. Rev. B **24**, 864 (1981), and references therein; M. Weinert, E. Wimmer, and A. J. Freeman, *ibid.* **26**, 4571 (1982); H. J. F. Jansen and A. J. Freeman, *ibid.* **30**, 561 (1984).

[21] D. M. Bylander and L. Kleinman, Phys. Rev. B **41**, 7868 (1990).

[22] A. Seidl, A. Görling, P. Vogl, J. A. Majewski, and M. Levy, Phys. Rev. B **53**, 3764 (1996).

[23] W. Wolf, E. Wimmer, S. Massidda, M. Posternak, and C. B. Geller, Bull. Am. Phys. Soc. **43**, 797 (1998).

[24] R. Asahi, W. Mannstadt, and A. J. Freeman, Phys. Rev. B **59**, 7486 (1999).

[25] C. B. Geller, W. Wolf, S. Picozzi, A. Continenza, R. Asahi, W. Mannstadt, A. J. Freeman, and E. Wimmer, Appl. Phys. Lett. **79**, 368 (2001).

[26] R. Asahi, W. Mannstadt, and A. J. Freeman, Phys. Rev. B **62**, 2552 (2000).

[27] L. Hedin and B. I. Lundqvist, J. Phys. C **4**, 2064 (1971).

[28] H. J. Monkhorst and J. D. Pack, Phys. Rev. B **13**, 5188 (1976).

[29] D. Jepsen and O. K. Andersen, Solid State Commun. **9**, 1763 (1971); G. Lehmann and M. Taut, Phys. Status Solidi B **54**, 469 (1972).

[30] S. Massidda, A. Continenza, A. J. Freeman, T. M. de Pascale, F. Meloni, and M. Serra, Phys. Rev. B **41**, 12 079 (1990).

[31] N. W. Ashcroft and N. D. Mermin, *Solid State Physics* (Holt, Rinehart and Winston, New York, 1976).

[32] T. Miyazaki and S. Adachi, Jpn. J. Appl. Phys., Part 1 **31**, 979 (1992).

[33] D. E. Aspnes and A. A. Studna, Phys. Rev. B **27**, 985 (1983).

[34] B. O. Seraphin and H. E. Bennett, in *Semiconductors and Semimetals*, edited by R. K. Wilardson and A. C. Beer (Academic, New York, 1967), Vol. 3, p. 499.

[35] M. Cardona, *Modulation Spectroscopy*, Solid State Physics Suppl. 11 (Academic, New York, 1969), pp. 55–65.

[36] J. Spitzer, A. Höpner, M. Kuball, M. Cardona, B. Jenichen, H. Neuroth, B. Brar, and H. Kroemer, J. Appl. Phys. **77**, 811 (1995).

[37] M. Muñoz, K. Wei, F. H. Pollak, J. L. Freeouf, and G. W. Charache, Phys. Rev. B **60**, 8105 (1999).

[38] S. Zollner, C. Lin, E. Schönherr, A. Böhringer, and M. Cardona, J. Appl. Phys. **66**, 383 (1989).